



Scalable green synthesis of hierarchically porous carbon microspheres by spray pyrolysis for high-performance supercapacitors

Jin Koo Kim¹, Yongju Yoo¹, Yun Chan Kang^{*}

Department of Materials Science and Engineering, Korea University, Anam-dong, Seongbuk-gu, Seoul 136-713, Republic of Korea



HIGHLIGHTS

- Hierarchically porous carbon microspheres are synthesized by spray pyrolysis.
- Carbonization during the spray pyrolysis is achieved without the heavy metal salt.
- Porosity and surface area can be tailored by adjusting the concentration of NaCl.
- Abundant micro/mesopores allow efficient ion transport with small ionic resistance.
- The synthesized carbon electrode exhibits enhanced performance as supercapacitor.

ARTICLE INFO

Keywords:

Spray pyrolysis
Hierarchical pore
Green synthesis
NaCl
Activated carbon
Supercapacitors

ABSTRACT

Designing carbon materials with optimized hierarchical pore structures is crucial to realize high-performance electrical double-layer capacitors (EDLCs) with enhanced energy and power densities. Therefore, the development of the suitable synthesis strategies for hierarchically porous carbon (HPC) materials with a higher productivity has attracted significant interest. Here, a facile, economic, scalable, and environmentally friendly method to synthesize hierarchical pore-structured carbon materials by spray pyrolysis without the use of heavy metal salts is presented. A spray solution containing sucrose, NaCl, and H₂SO₄ is aerosolized by an ultrasonic nebulizer and undergoes pyrolysis to produce NaCl-templated carbon microspheres, followed by an activation step and washing to obtain HPC. Endowed with a specific surface area up to 1704 m² g⁻¹ and pore volume of 1.81 cm³ g⁻¹, the resulting carbon contains an interconnected micro/mesoporous network, which provides efficient ion transport channels with a short diffusion length and small ionic resistance. Moreover, it exhibits a specific capacitance of 102 F g⁻¹ at a current density of 30 A g⁻¹ with a retention of 92% over 10,000 cycles at 10 A g⁻¹ as an electrode in an organic-electrolyte-based EDLC. In contrast, the sheer microporous carbon does not exhibit EDLC behavior at a high rate. The proposed synthesis technique paves the way for cheap scalable syntheses of carbon materials with desired pore structures by spray pyrolysis, which may inspire further studies for various applications including energy storage, where carbon materials with high specific surface areas and yields are of significance.

1. Introduction

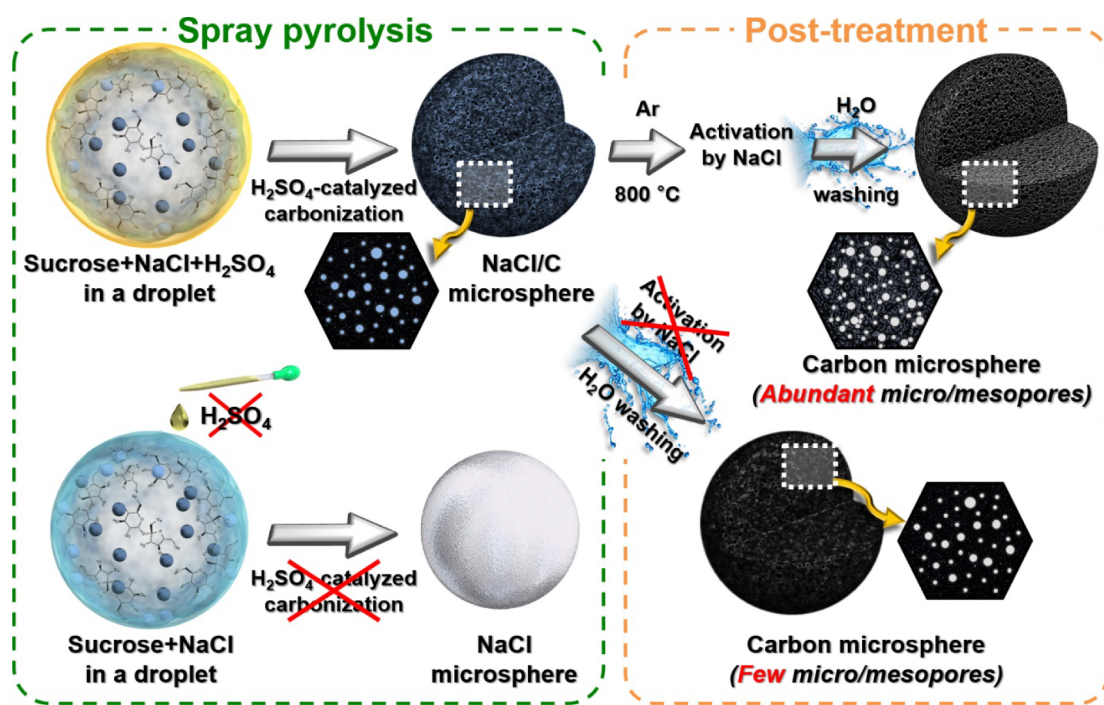
Electrical double-layer capacitors (EDLCs), referred to as supercapacitors, have attracted tremendous attention as supplements for the next-generation energy storage devices owing to their high power densities and ultralong cycling lifetimes [1–5]. However, the low energy density of EDLC, compared with that of lithium-ion battery, should be improved for applications in daily life [3–8]. The EDLC stores energy by charge separation through physical adsorption/desorption of

electrolyte ions at the interface of carbon electrodes [9–11]. Therefore, a carbon material with a high specific surface area (SSA) should be utilized as the electrode to significantly improve the capacitance. Commercially available activated carbons that exhibit a high SSA (< 3000 m² g⁻¹) with a large number of micropores (pore width smaller than 2 nm) have been utilized as electrodes for supercapacitors. However, their pore structure results in a long ion pathway and severely hinders the ion diffusion, leading to poor charge storage capability at high rates [11–13]. For this reason, synthesis of porous carbon

* Corresponding author.

E-mail address: yckang@korea.ac.kr (Y.C. Kang).

¹ These authors contributed equally to this work.



Scheme 1. The synthesis procedure of the NaCl-activated carbon microsphere via spray pyrolysis and post-treatment.

materials with appropriate pore size has gained great research interests [11–17]. In contrast to the micropores, mesopores (pore width of 2–50 nm) can act as ion highway that facilitates fast ion diffusion [4]. However, mesopores provide limited contribution to the capacitance and give rise to a large pore volume, leading to low energy density [4,11]. Therefore, it is highly desirable to incorporate mesopores into the microporous carbon material so as to bring a considerable enhancement in both the energy and power densities [11–17].

In this regard, various carbon materials with hierarchical pore structures suitable for organic electrolytes have been developed [17–20]. For example, Gogotsi's group developed various types of carbide-derived carbons by selective removal of metals or metalloid atoms from carbide precursors [18]. Fuertes et al. synthesized hierarchical micro/mesoporous carbon nanosheets with a high SSA ($1890 \text{ m}^2 \text{ g}^{-1}$) through carbonization of sodium gluconate followed by an additional activation step [19]. Wang et al. synthesized interconnected partially graphitic carbon nanosheets with a high SSA of $2287 \text{ m}^2 \text{ g}^{-1}$ using the hydrothermal method and activation process [20]. In addition, carbon materials based on biomass, carbon nanotubes, graphene, and carbon fibers have been widely studied; they exhibited high SSAs with suitable pore structures [21–29]. Nevertheless, most synthesis methods are inadequate for commercial supercapacitors owing to the complexity of the entire process, high cost, and difficulty in mass production. Therefore, development of a cost-effective, simple, and large-scale synthesis method to produce carbon materials with hierarchical pore structures is required.

Recently, spray pyrolysis has emerged as an important technique for syntheses of various nanostructured materials owing to its feasibility, scalability and cost-efficiency [30–33]. Several studies have been carried out to synthesize carbon materials as electrodes for supercapacitors by spray pyrolysis [34–41]. Jang's group reported the fabrication of crumpled graphene balls by spray pyrolysis of graphene oxide colloidal solution [37]. It exhibited a specific capacitance of 156 F g^{-1} at 0.1 A g^{-1} in an aqueous electrolyte. The same group also introduced the 3D network-structured crumpled graphene/carbon nanotube/polyaniline composite using the same method, which exhibited greatly enhanced specific capacitance up to 295 F g^{-1} [38]. Wang et al. fabricated microporous carbon microspheres with a high SSA ($1106 \text{ m}^2 \text{ g}^{-1}$) using

ZnO as a porogen [39]. Although a high specific capacitance (112 F g^{-1} at 0.5 A g^{-1}) was achieved in an aqueous electrolyte, it was still far from satisfactory in terms of energy density owing to the low voltage window ($< 1 \text{ V}$). Sun et al. reported synthesis of a N-doped porous carbon sphere from a copolymer of melamine, phenol, and formaldehyde with silica as a pore template, which had a high SSA of $1519 \text{ m}^2 \text{ g}^{-1}$ [40]. Yoo et al. synthesized carbon microspheres with a multimodal pore size distribution (large number of micropores and small number of mesopores) by etching vanadium oxide nanocrystals, which exhibited a high specific capacitance (110 F g^{-1} at 30 A g^{-1}) and long cycling life over 10,000 cycles in an organic electrolyte [41]. According to the previous studies, no carbon microspheres could be produced by spray pyrolysis of carbon-source-containing solutions without assistance of heavy metal salts, which catalyze the carbonization reaction [34–36,39–41]. However, the use of heavy metal salts to produce carbon microspheres entails an etching process of the metal species to generate porosity, which inevitably requires harsh solvents and thus increases the cost and complexity of the process. Graphene and carbon nanotube-based materials showed promising performances, but they had to be acid-treated before use to achieve good dispersion in water for aerosol formation [36–38]. Although there have been a few reports that utilized alkali salts as pore templates [42–48], most of them relied on the use of sodium carbonate or bicarbonate that act as basic catalysts for carbonization, without which no carbon microsphere was produced [44–47]. In addition, the proposed methods were not appropriate to create suitable pore structures for application in supercapacitors [47,48]. Therefore, a more flexible, economic, and environmentally friendly route to synthesize carbon materials by spray pyrolysis should be studied.

With all these comprehensive considerations in mind, we report a simple scalable synthesis of hierarchically porous carbon (HPC) microspheres by spray pyrolysis using inexpensive reagents, i.e., sugar (sucrose; $\text{C}_{12}\text{H}_{22}\text{O}_{11}$), sulfuric acid (H_2SO_4), and salt (sodium chloride; NaCl). Inspired from the “carbon snake experiment”, a well-known school experiment in which the dehydration reaction of sucrose by sulfuric acid is utilized to produce a stick of carbon, we came up with an idea of using sulfuric acid to catalyze the carbonization of sucrose during the spray pyrolysis. NaCl, which is widely used to produce

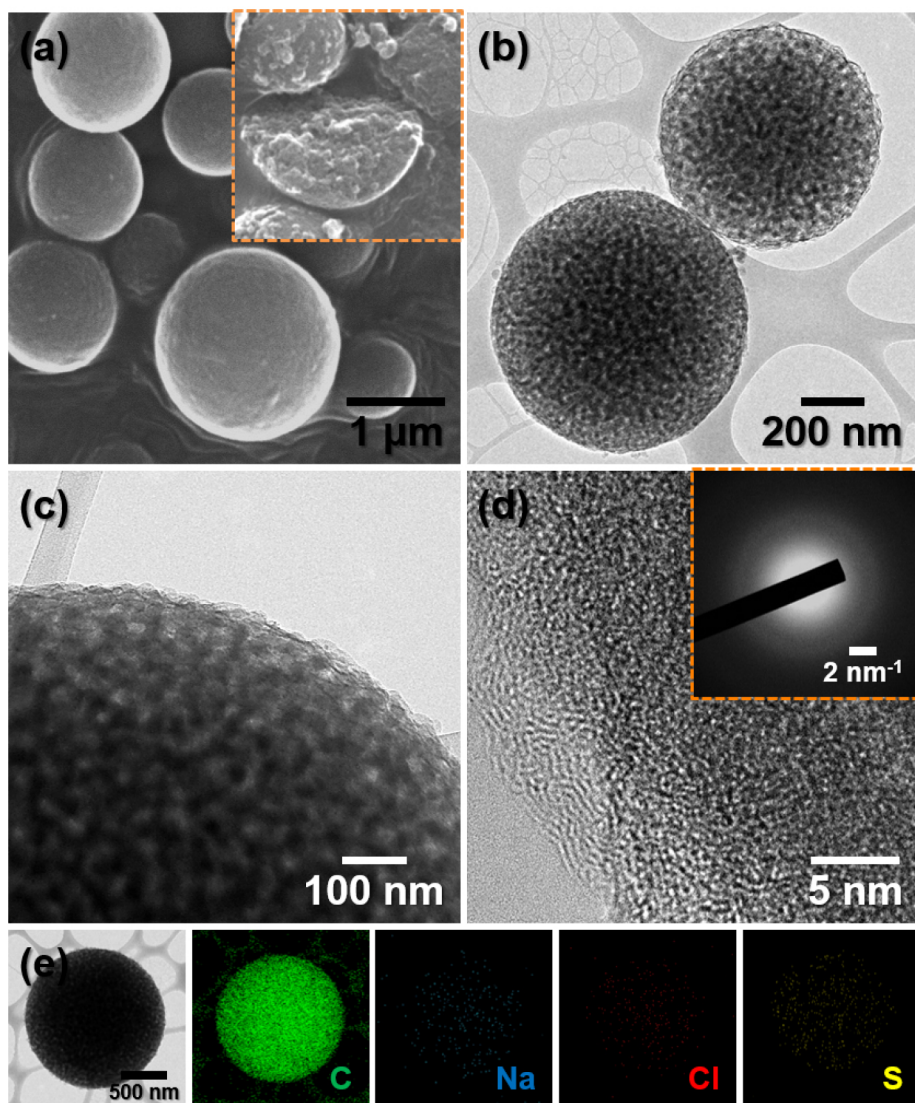


Fig. 1. Morphological and structural characterizations of C-SP: (a) SEM image, (b,c) TEM images, (d) HR-TEM image and (inset) SAED pattern, and (e) elemental mapping images.

porous nanostructures [49–52], was applied as a pore template and activating agent. The entire process is simple and environmentally benign, as it employs only water-soluble precursors and template. The ratio between the numbers of micropores and mesopores of the synthesized carbon microspheres could be easily controlled by adjusting the amount of NaCl with respect to that of sucrose in the spray solution. The resulting HPC microspheres were endowed with a very high SSA and optimized pore structure for an organic-electrolyte-based supercapacitor. The proposed synthesis technique paves the way for cheap scalable syntheses of HPC materials by spray pyrolysis, which may be an inspirational protocol for further applications including energy storage, where carbon materials with high SSAs and yields are of significance.

2. Experimental section

2.1. Synthesis of NaCl-activated carbon microspheres

The NaCl-activated carbon microspheres were synthesized using a transparent aqueous spray solution (250 mL) containing sodium

chloride (NaCl; Junsei, 99%), sucrose ($C_{12}H_{22}O_{11}$; Junsei), and sulfuric acid (H_2SO_4 ; Samchun, 95%). The amount of sodium chloride was varied (0.2–0.4 mol L⁻¹). The amounts of sucrose and sulfuric acid were fixed to 0.2 and 0.5 mol L⁻¹, respectively. The solutions were atomized by an ultrasonic nebulizer and blown into a quartz reactor (length: 1200 mm; diameter: 50 mm) with N₂ gas at a flow rate of 5 L min⁻¹. The temperature of the furnace was 900 °C. The powders were collected and post-treated at 800 °C under Ar flow for 3 h. After cooling down to room temperature within the furnace, the powders were immersed in distilled water under mild stirring for 1 h to remove NaCl and byproducts. The powders were then filtered and washed with a copious amount of water, followed by vacuum drying. For comparison, carbon microspheres were prepared in the same manner without addition of NaCl in the spray solution.

2.2. Characterizations

A morphological characterization was carried out by scanning electron microscopy (SEM; TESCAN, VEGA3) and field-emission transmission electron microscopy (TEM; JEOL, JEM-2100F). X-ray

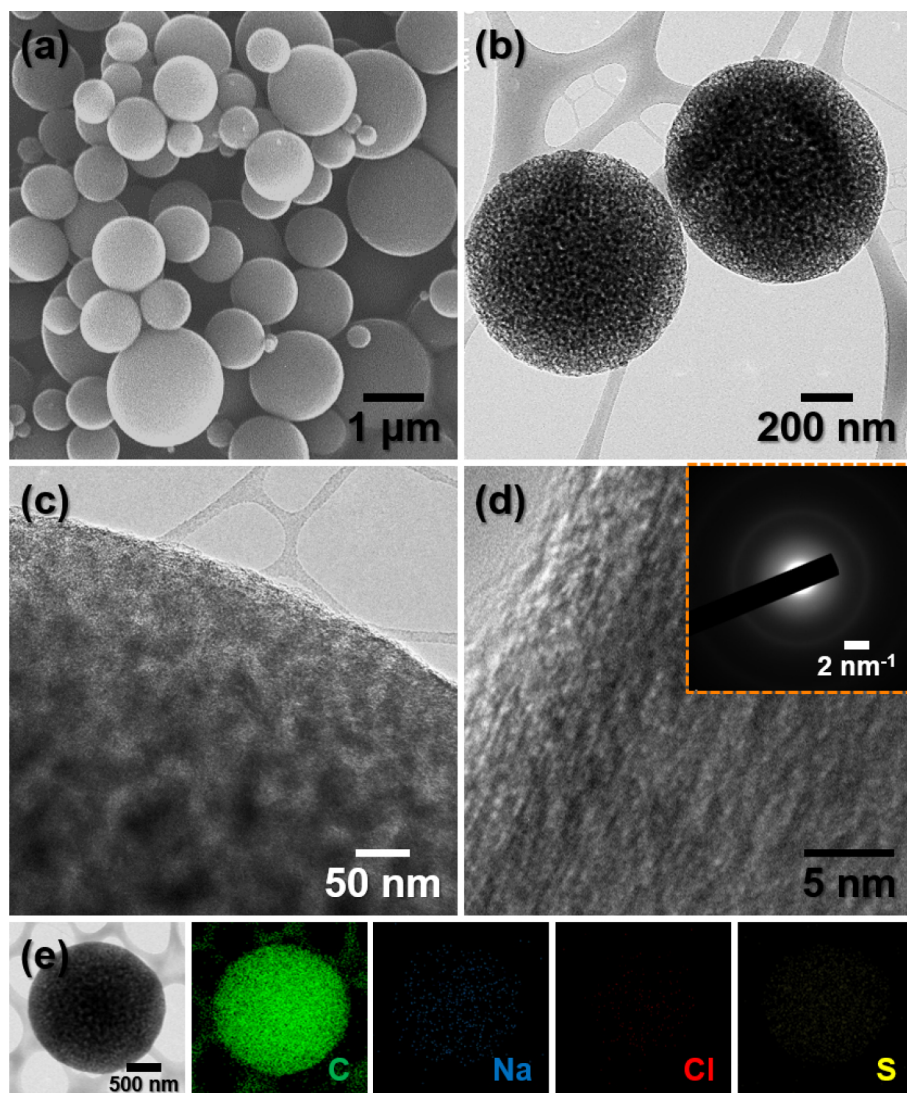


Fig. 2. Morphological and structural characterizations of HPC: (a) SEM image, (b,c) TEM images, (d) HR-TEM image and (inset) SAED pattern, and (e) elemental mapping images.

diffractometry (XRD; X'pert PRO MPD) with Cu K α radiation ($\lambda = 1.5418 \text{ \AA}$) was carried out at the Korea Basic Science Institute (Daegu). Raman spectroscopy (LabRam HR800, Horiba Jobin-Yvon, excited by a 515-nm diode laser) was carried out at room temperature to analyze the carbon structures in the samples. X-ray photoelectron spectroscopy (XPS; Thermo Scientific K-Alpha, focused by a monochromatic Al K α radiation) at 12 kV and 20 mA was used to evaluate the chemical environments of the samples. N₂ adsorption-desorption isotherms of the samples were obtained using a TriStar 3000 analyzer and 3Flex 3500 at 77 K. The SSAs of the samples were measured by Brunauer-Emmett-Teller (BET) method, while the pore size distributions were characterized by the Barrett-Joyner-Halenda (BJH) and Horvath-Kawazoe (HK) methods. The thermogravimetric analysis (TGA; SDT Q600) of the samples was performed in the range of 25–800 °C at a ramping rate of 5 °C min⁻¹ under air.

2.3. Electrochemical measurements

The electrochemical properties of the samples were analyzed by assembling 2032-type coin cells with a two-electrode system in an Ar-

filled glove box. The electrodes were prepared by printing water-based slurries of mixtures of the samples (active material; 80 wt%), Super P® (conducting agent; 10 wt%), and sodium carboxymethyl cellulose (binder; 10 wt%) on Al foils. After desiccation in a vacuum oven, the electrode was cut into disks with diameters of 1.4 cm. The loading mass on a single disk electrode was approximately 1.9 mg. The electrolyte was prepared by dissolving 1 mol L⁻¹ of tetraethylammonium tetrafluoroborate in acetonitrile (TEABF₄/AN). A microporous polypropylene film was used as the separator. The cyclic voltammetry (CV) and galvanostatic charge-discharge (GCD) measurements were carried out in the range of 0–2.5 V. The electrochemical impedance spectroscopy (EIS) measurements at 10 mV (AC) were performed in the frequency range of 0.01 Hz–100 kHz.

3. Results and discussion

The synthesis procedure of the NaCl-activated carbon microsphere is depicted in Scheme 1. Mist of droplets atomized from a transparent aqueous solution containing NaCl, sucrose, and sulfuric acid flows into a quartz reactor (900 °C) with N₂ carrier gas. The heat from the reactor

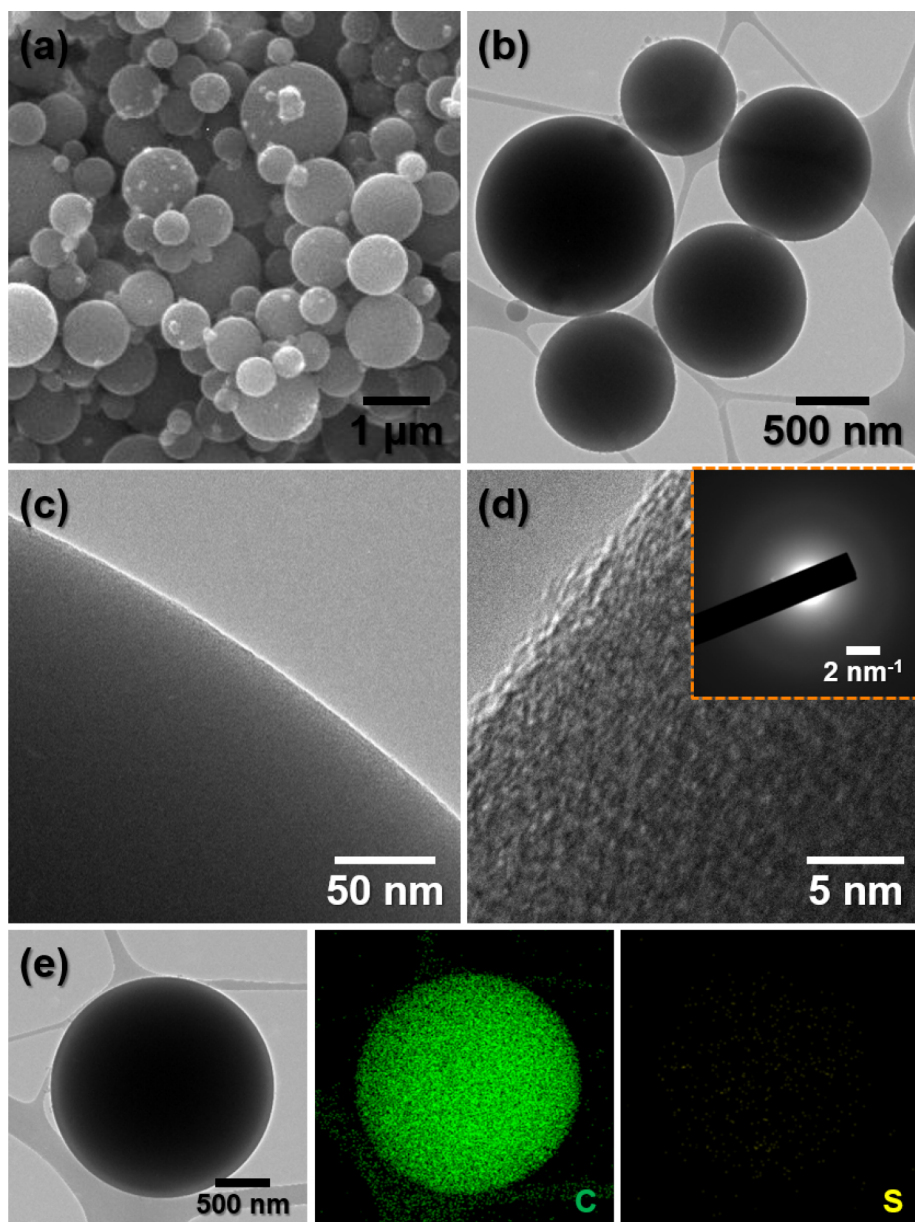


Fig. 3. Morphological and structural characterizations of SC-SP: (a) SEM image, (b,c) TEM images, (d) HR-TEM image and (inset) SAED pattern, and (e) elemental mapping images.

rapidly vaporizes the water in the droplets. In addition, as the temperature of the reactor is sufficiently high, the decomposition of sucrose and melting of NaCl occur simultaneously, forming an intermediate microsphere of molten NaCl around which the sucrose-derived carbon atoms are networked. As soon as the microsphere passes by the hot zone of the reactor and cools down, the NaCl in the microsphere recrystallizes throughout the carbon matrix, forming a NaCl/carbon composite microsphere. When the in-situ-formed solid NaCl template is washed away with distilled water, the micro/mesoporous network is created throughout the carbon matrix. If the NaCl/carbon composite microsphere is post-treated under Ar atmosphere at 800 °C, NaCl nanocrystals activates the surrounding carbon matrix, which in turn yields HPC microspheres with abundant micropores and mesopores after the removal of NaCl. It is worth noting that the carbonization of sucrose is catalyzed by the violent dehydration reaction by sulfuric acid during

the spray pyrolysis. This was experimentally confirmed by spray pyrolysis of the same solution without sulfuric acid, which did not produce the carbon product. The array of the as-prepared powders in Fig. S1 shows obvious color contrast, which reflects the presence of carbon. This implies that NaCl alone was unable to catalyze the dehydration and carbonization of sucrose, as it was chemically inert under the proposed synthetic condition, which is in agreement with the discussions in the previous reports [39,47,48,53,54]. Nearly 10 g of NaCl/carbon composite precursor powder could be produced within 3 h. Therefore, the daily laboratory-scale production rate was 80 g per day.

The SEM images of the as-prepared NaCl/carbon composite microspheres synthesized by spray pyrolysis (NaCl/C-SP) are presented in Fig. S2. The NaCl nanocrystals dispersed throughout the carbon microspheres are clearly discernable. A part of NaCl was flowed out of the carbon microsphere and underwent crystal growth during the synthesis,

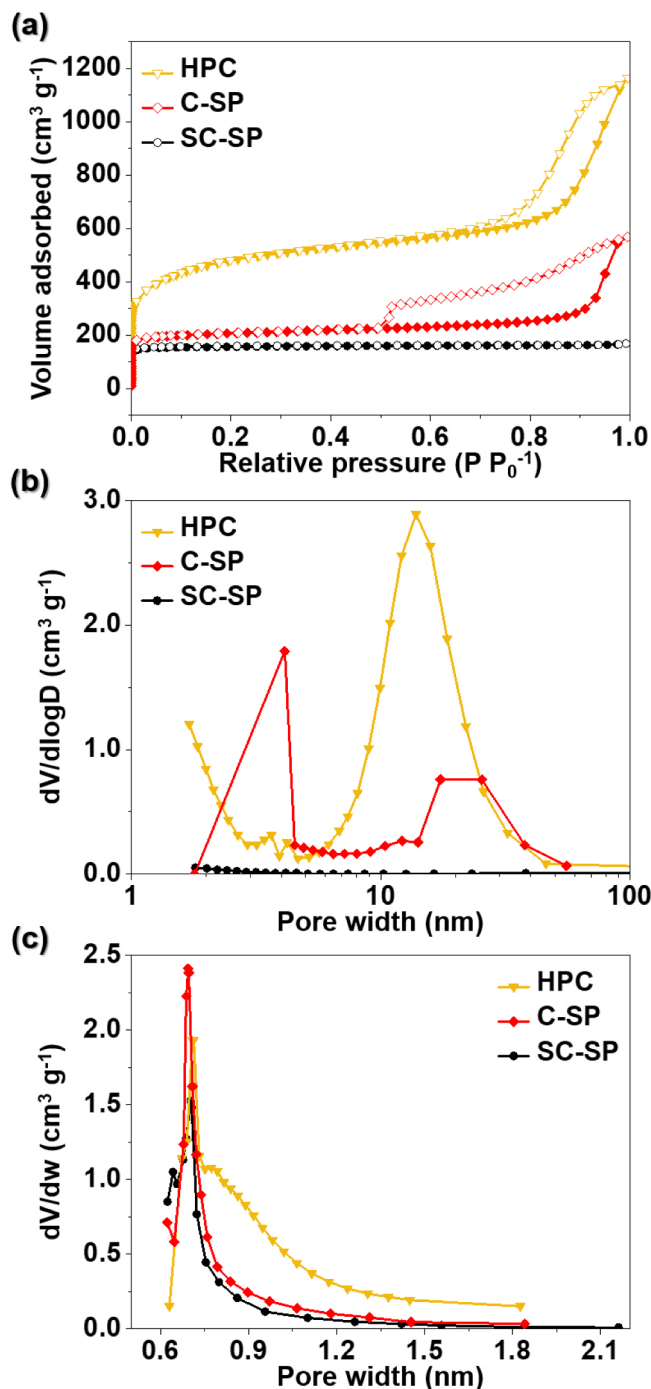


Fig. 4. (a) N₂ gas adsorption-desorption isotherm curves, (b) BJH pore size distributions, and (c) Horvath-Kawazoe differential pore volume plots of SC-SP, C-SP, and HPC.

as reflected in the formation of non-spherical particles. The morphology of the carbon microspheres after the removal of NaCl by washing (C-SP) is shown in Fig. 1. The SEM image in Fig. 1a shows the pore formation along the surface. The shattered microsphere image in the inset confirms the formation of an internal mesoporous network, indicating the homogeneous distribution of NaCl throughout the carbon matrix before the removal. The externally exposed NaCl nanocrystals, which could be observed as non-spherical particles in Fig. S2, were completely eliminated. The TEM image in Fig. 1b shows the well-developed internal

pore structure of C-SP. The high-resolution TEM images in Fig. 1c and d suggest that the carbon matrix is predominantly amorphous, which is also indicated by the blurry ring in the selected-area electron diffraction (SAED) pattern in the inset of Fig. 1d. As shown in the elemental maps (Fig. 1e), C-SP does not exhibit Na and Cl components. The purity of C-SP was confirmed by an XRD pattern, as shown in Fig. S3 along with that of NaCl/C-SP for comparison. The XRD pattern of NaCl/C-SP shows prominent peaks corresponding to (1 1 1), (2 0 0), (2 2 0), (2 2 2), and (4 0 0) planes of the cubic NaCl and miscellaneous peaks for orthorhombic sodium sulfate, which might have been produced by the reaction between sulfuric acid and NaCl. On the other hand, the XRD pattern of C-SP does not contain peaks from NaCl and sodium sulfate, demonstrating that the salts in C-SP were completely washed away by the water.

The morphologies of the HPC microspheres obtained after the activation of NaCl/C-SP are presented in Figs. S4 and 2. The SEM image (Fig. S4) obtained after the activation is not significantly different from that of NaCl/C-SP. The XRD pattern of the activated NaCl/C-SP in Fig. S5a indicates the formation of NaCl-derived byproducts, which are all soluble in water. The SEM and TEM images of HPC in Fig. 2a and b, respectively, show the homogeneous distribution of pores throughout the microspheres after washing away the NaCl and byproducts from the activated NaCl/C-SP. The high-resolution TEM images in Fig. 2c and d reveal the formation of a highly micro/mesoporous network. The SAED ring in the inset of Fig. 2d is similar to that of C-SP (inset of Fig. 1d), suggesting a locally disordered structure of carbon. As confirmed by the elemental maps (Fig. 2e) and XRD pattern (Fig. S5a), HPC contains only carbon. The purity of carbon was further corroborated by a TGA under air, as shown in Fig. S6. The initial weight loss of 2.6% was attributed to the vaporization of adsorbed water molecules. The combustion of carbon is indicated by the abrupt weight loss from 480 °C. The curve at the end shows a weight loss of 99.6%, suggesting that HPC is virtually free of impurities.

In order to investigate the role of NaCl in the porosity of the carbon microspheres, spray pyrolysis and subsequent heat treatment of the solution without NaCl were carried out. The SEM and TEM images in Fig. 3a and b show the formation of solid carbon microspheres (SC-SP), respectively. Porous network was not observed even in the high-resolution TEM images in Fig. 3c and d. Therefore, it could be inferred that NaCl is indispensable for the creation of the pore structure. The SAED pattern in the inset of Fig. 3d indicates that the carbon is amorphous. The elemental maps in Fig. 3e signify that the sulfuric acid was completely decomposed after the catalysis of the carbonization of sucrose.

The porosities of the samples were further analyzed by the N₂ adsorption method. The N₂ adsorption/desorption isotherms of C-SP and HPC in Fig. 4a were close to the combined form of type I and IV isotherms with typical H3 hysteresis loops, according to the International Union of Pure and Applied Chemistry (IUPAC) classification. It is worth noting that the isotherm of HPC exhibited a sharper increase of N₂ uptake at the low-relative-pressure region ($P/P_0 < 0.01$) than that of C-SP, which implies the creation of a significantly larger number of micropores in HPC after the activation of C-SP [55–57]. The large hysteresis loops extending from the medium-relative-pressure region are associated with the capillary condensation in the mesopores [55]. These results strongly indicate the coexistence of micropores and mesopores in C-SP and HPC, confirming the formation of the hierarchical pore structure in the microspheres by the introduction of NaCl. On the other hand, the isotherms of SC-SP could be classified as type I, exhibiting a completely different trend. Initially, a sharp N₂ uptake was observed, which then approached a limiting value, reflecting the sheer microporosity. For a quantitative analysis, the SSAs of the samples were derived by the BET method. The BET SSAs of SC-SP, C-SP, and HPC were 627, 804, and 1704 m² g⁻¹, respectively. The size distributions of

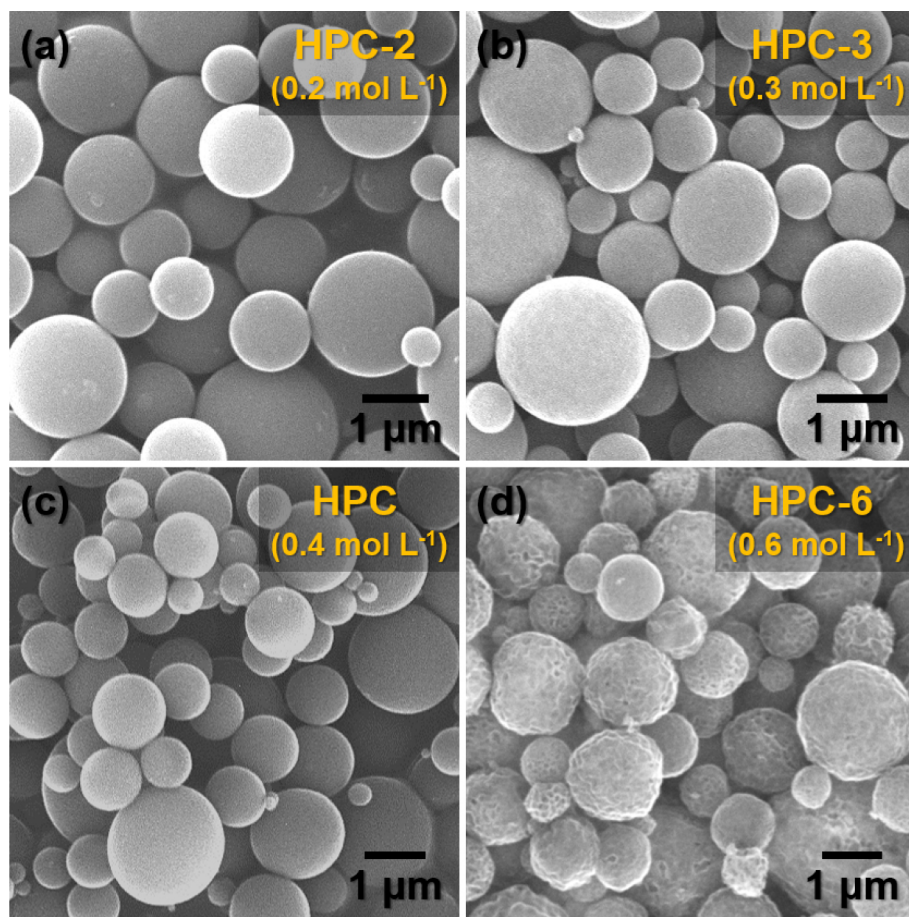


Fig. 5. SEM images of the carbon microspheres prepared with different NaCl concentrations: (a) 0.2 mol L^{-1} , (b) 0.3 mol L^{-1} , (c) 0.4 mol L^{-1} , and (d) 0.6 mol L^{-1} .

the mesopores in C-SP and HPC were calculated by the BJH method, as shown in Fig. 4b. The average mesopore size of C-SP was 6.9 nm, which increased up to 7.6 nm after the activation. The micropore distributions of the samples were estimated by the HK method, as shown in Fig. 4c. SC-SP and C-SP had narrow distributions in the range of 0.6–0.9 nm with a sharp maximum at 0.70 nm, whereas HPC had a relatively broad distribution. The micropore volumes of SC-SP, C-SP, and HPC were 0.25, 0.28, and $0.66 \text{ cm}^3 \text{ g}^{-1}$, respectively, as determined by a *t*-plot calculation. As they had total pore volumes of 0.26, 0.88, and $1.81 \text{ cm}^3 \text{ g}^{-1}$, the proportions of micropores to the total porosity were determined to be 96, 32, and 37%, respectively. According to the results of the N_2 adsorption analysis, HPC exhibits a very high SSA and well-developed hierarchical porosity, which are crucial to accelerate the electrolyte access to the micropores for rapid adsorption/desorption of the electrolyte ions. The porosity of the carbon could be tailored by adjusting the concentration of NaCl with respect to that of sucrose. The SEM images in Fig. 5 show the morphologies of the carbon microspheres prepared in the same manner with different NaCl concentrations (denoted as HPC-2, HPC-3, HPC, and HPC-6). Although no marked differences were observed between their morphologies, significant differences were observed between their isotherms, as shown in Fig. 6. With the increase in the concentration of NaCl, the isotherms approached the combined form of types I and IV from type I (Fig. 6a), indicating the increasing predominance of mesoporosity over microporosity. In the case of HPC-6, a relatively sharp increment of the N_2 adsorption at $P/P_0 > 0.9$ was observed, indicating the emergence of macroporosity. In addition, the average diameters of the mesopores and

micropores increased correspondingly (Fig. 6b and c). The BET SSAs, pore volumes, and pore diameters of the samples are summarized in Table 1.

The carbon structures of the samples were characterized by Raman spectroscopy and XPS. The Raman spectra of C-SP and HPC in Fig. 7a show two noticeable peaks at ~ 1348 and 1593 cm^{-1} , which correspond to the D and G bands of the carbon, respectively. The D band emerges from disordered sp^3 carbon, while the G band is a feature of sp^2 carbon from graphite [58–60]. The peak intensity ratio between the D and G bands (I_D/I_G) can reveal the degree of order of the carbon. The I_D/I_G ratios of C-SP and HPC were 0.90 and 0.99, respectively, indicating that the activation process oxidized the carbon atoms and introduced more defects in HPC [58]. The XPS survey spectra of C-SP and HPC in Fig. 7b show C and O components. Signals from Na, Cl, and S were not detected, which is consistent with the elemental maps and TGA results. The C 1s spectra of C-SP and HPC in Fig. 7c and d show peaks at 284.4, 285.5, 286.3, 288.4, and 291.3 eV, corresponding to $\text{C}=\text{C}$ (sp^2), $\text{C}-\text{C}$ (sp^3), $\text{C}-\text{O}$, $\text{C}=\text{O}$, and $\pi-\pi^*$, respectively [41,61,62]. Note that the portion of $\text{C}-\text{C}$ (sp^3) peak in HPC was more pronounced compared with that of C-SP. This indicates that the activation process increased defects in HPC to some extent, which accords with the result from Raman spectroscopy.

The electrochemical properties of the samples in supercapacitors were evaluated using an organic electrolyte (1 mol L^{-1} TEABF₄/AN) with a two-electrode system by assembling 2032-type coin cells. CV and GCD curves of HPC and C-SP are compared in Fig. 8. HPC exhibited an enhanced specific capacitance (C_{sp}) over a wide voltage window of

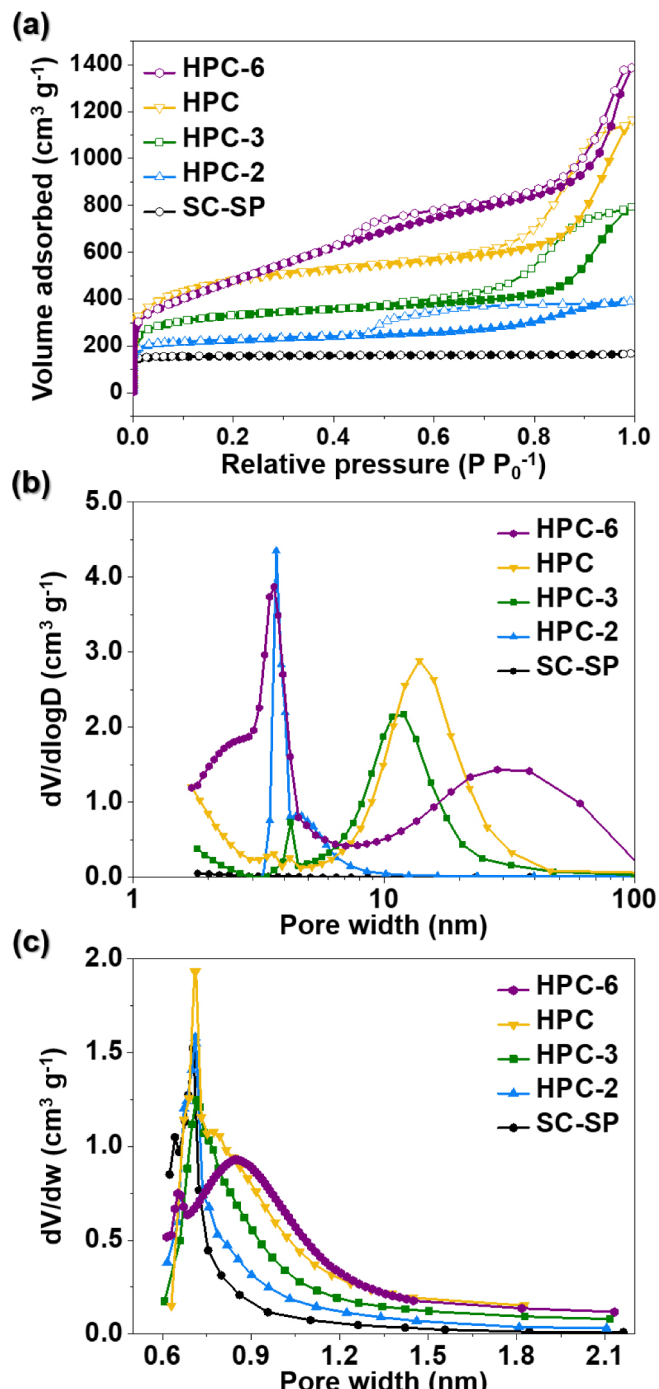


Fig. 6. (a) N₂ gas adsorption-desorption isotherm curves, (b) BJH pore size distributions, and (c) Horvath-Kawazoe differential pore volume plots of SC-SP, HPC-2, HPC-3, and HPC.

2.5 V (Fig. 8a) compared with that of C-SP (Fig. 8b), suggesting that more energy could be stored in HPC than in C-SP. In addition, the CV curves of HPC had nearly rectangular shapes without substantial distortions even at a high scan rate of 500 mV s⁻¹, indicating that HPC had a typical EDLC behavior with an excellent rate capability. This was further confirmed by plotting the C_{sp} values derived from the CV curves of HPC and C-SP at different scan rates, as shown in Fig. 8c. When the scan rate was increased from 50 to 500 mV s⁻¹, C_{sp} of HPC was maintained in the range of 100–87 F g⁻¹. To investigate the effect of the

porosity on the EDLC behavior, the CV curves of HPC were compared with those of SC-SP, HPC-2, and HPC-3, as shown in Fig. S7. The C_{sp} increased as the concentration of NaCl increased from 0 (SC-SP) to 0.4 mol L⁻¹ (HPC). It is worth noting that SC-SP did not exhibit EDLC behavior (Fig. S7a). As shown by the N₂ adsorption/desorption isotherms in Fig. 4a, SC-SP had sheer micropores. Even though the micropores can provide a large surface area to ensure a high energy storage, they provide a limited contribution to the capacitance at high rates unless they are interconnected with mesopores, which can play an essential role for the promotion of the electrolyte ion diffusion kinetics [11,13,55,63]. As 96% of the porosity of SC-SP corresponded to micropores, most of them were not accessible to the electrolyte ions, thus leading to an extremely low capacitance. The introduction of NaCl and subsequent activation increased the contents of both micropores and mesopores, thus increasing the electrolyte-accessible surface area. Therefore, the C_{sp} values of the samples exhibited an increasing tendency with the concentration of NaCl (Figs. S7b-d). However, HPC-6 (0.6 mol L⁻¹) did not exhibit EDLC behavior, as witnessed by off-rectangular form of the curve (Fig. S8a). As a matter of fact, the electrochemical properties of HPC-6 could not be characterized properly. As HPC-6 was determined to be more macroporous, the powder was much lighter than any other sample. Therefore, the binder material (sodium carboxymethyl cellulose) could not effectively hold HPC-6 powder within the electrode, resulting in delamination after drying (Fig. S8b). Although the CV test was conducted with the electrodes with minimum delamination, poor electrical contact between the current collector (Al foil) and the active material (HPC-6) resulted in serious leakage current. Therefore, the optimized EDLC performance was achieved at 0.4 mol L⁻¹ of NaCl. The superior electrochemical properties of HPC were also confirmed by GCD curves. The GCD curves of HPC in Fig. 8d are almost linear and symmetrical with a minor internal resistance (iR) drop (0.06 V at 1 A g⁻¹), indicating a good capacitive performance. In contrast, the GCD curves of C-SP (Fig. 8e) show a significant iR drop (0.24 V at 1 A g⁻¹). The superior rate performance of HPC to that of C-SP is shown in Fig. 8f. C_{sp} of HPC slightly decreased from 115 to 102 F g⁻¹ (retention: 89%) even when the current density significantly increased from 1 to 30 A g⁻¹, whereas that of C-SP significantly decreased from 43 to 30 F g⁻¹ (retention: 70%). EIS was performed to further evaluate the performance of HPC. The Nyquist plots of HPC and C-SP in Fig. 8g show almost vertical lines in the low-frequency region, which demonstrate the ideal capacitive behavior [64,65]. The inset of Fig. 8g, a magnified view of the high-frequency region, shows the transition from the semicircle to the vertical line. It is worth noting that the projected lengths of the 45° lines in the medium-frequency region on the real axis, associated with the resistance from the ion diffusion into the electrode, were extremely small, indicating that the pore structures of both HPC and C-SP were suitable for the rapid ion transport. The equivalent series resistance (ESR), composed mainly of ionic, electrode, and contact resistances, can be obtained by extrapolating the vertical line to the real axis [64–66]. The ESRs of HPC and C-SP were 3.07 and 5.0 Ω, respectively. These results are consistent with the lower iR drop of HPC than that of C-SP observed in the GCD curves in Fig. 8d and e. The significantly lower ESR of HPC can be attributed to its well-developed hierarchical open pore structure, whose interconnected micro/mesopores provide efficient ion transport channels with a short diffusion length and small ionic resistance [13,64]. The C_{sp} -frequency plots in Fig. 8h also show that HPC exhibits higher capacitance value than C-SP at all frequency region. At high frequency region (50 Hz), the capacitance values of HPC and C-SP were 46.8 and 8.1 F g⁻¹, respectively. Similarly, at low frequency region (10⁻² Hz), HPC exhibited higher capacitance value (95.8 F g⁻¹) than C-SP (27.0 F g⁻¹). This result corresponds to the investigations in Fig. 8d-f. HPC also exhibited a remarkable cycling stability with a retention of 89% of the initial C_{sp} after 10,000 cycles at a high current density of 2 A g⁻¹, as shown in

Table 1

Textural properties of the carbon microspheres prepared with different conditions.

Sample	$S_{\text{BET}}^{\text{a)}$ ($\text{m}^2 \text{g}^{-1}$)	$V_{\text{tot}}^{\text{b)}$ ($\text{cm}^3 \text{g}^{-1}$)	$V_{\text{mic}}^{\text{c)}$ ($\text{cm}^3 \text{g}^{-1}$)	$V_{\text{mes}}^{\text{d)}$ ($\text{cm}^3 \text{g}^{-1}$)	$D_{\text{avg}}^{\text{e)}$ (nm)
SC-SP	627	0.26	0.25	0.01	1.67
C-SP	804	0.88	0.28	0.60	4.39
HPC	1704	1.81	0.66	1.15	4.24
HPC-2	852	0.61	0.28	0.33	2.84
HPC-3	1205	1.23	0.45	0.78	4.09
HPC-6	1725	2.15	0.84	1.31	4.98

a) BET specific surface area;

b) total pore volume determined at $p/p_0 \sim 0.95$;

c) micropore volume estimated by t-plot;

d) mesopore volume determined by the difference between V_{tot} and V_{mic} ;

e) average pore diameter calculated by $4V_{\text{tot}}/S_{\text{BET}}$.

Fig. 8i. This indicates the stable charging and discharging processes of the HPC electrodes at an operating voltage window of 2.5 V with minimal side reaction [67]. In addition, the Coulombic efficiencies of HPC and C-SP were measured to be as high as 98.5% and 99.4% after 10,000 cycles, respectively, which accord with the standard of EDLCs based on porous carbon and 1 M TEABF₄/AN [68,69].

To evaluate the overall performances of our samples, the energy and power densities of HPC and C-SP were calculated and presented on the Ragone plot in Fig. 9. HPC exhibited a higher maximum power density (47.1 kW kg^{-1}) along with a higher maximum energy density (24.9 Wh kg^{-1}) than those of C-SP. The power and energy densities of HPC were comparable to those of previously reported carbon materials, as summarized in Table S1. For example, the energy density of HPC is

comparable to those of polysiloxane-derived carbon (31 Wh kg^{-1}) [57], shiitake mushroom-derived carbon (18 Wh kg^{-1}) [58], and macropore-rich activated carbon (10 Wh kg^{-1}) [70]. This implies that the carbon material having a high SSA with the optimized hierarchical pore structure is promising for the development of high-performance EDLCs.

4. Conclusion

We proposed a facile, economic, scalable, and environmentally friendly synthesis strategy for HPC materials containing interconnected micro/mesoporous networks by spray pyrolysis and subsequent activation process. The carbonization of sucrose could be successfully catalyzed by the violent dehydration reaction by sulfuric acid during the spray pyrolysis. This is a very promising approach to synthesize carbon materials by spray pyrolysis, which is different from the conventional method using heavy metal salts to catalyze the carbonization that requires etching with harsh solvents. NaCl, which was added together with sucrose and sulfuric acid, acted as an in-situ-formed pore template and activating agent. The resulting carbon materials with hierarchical pore structures exhibited high SSAs and pore volumes. The porosity could be tailored by adjusting the NaCl concentration. The interconnected micro/mesoporous network maximized the electrolyte-accessible surface area and provided efficient ion transport channels with a short diffusion length and small ionic resistance. The structure exhibited an excellent rate performance at a high current density of 30 A g^{-1} as well as comparable power and energy densities. Our method can be thoroughly employed for various applications including energy storage, where carbon materials with high SSAs and yields are of significance.

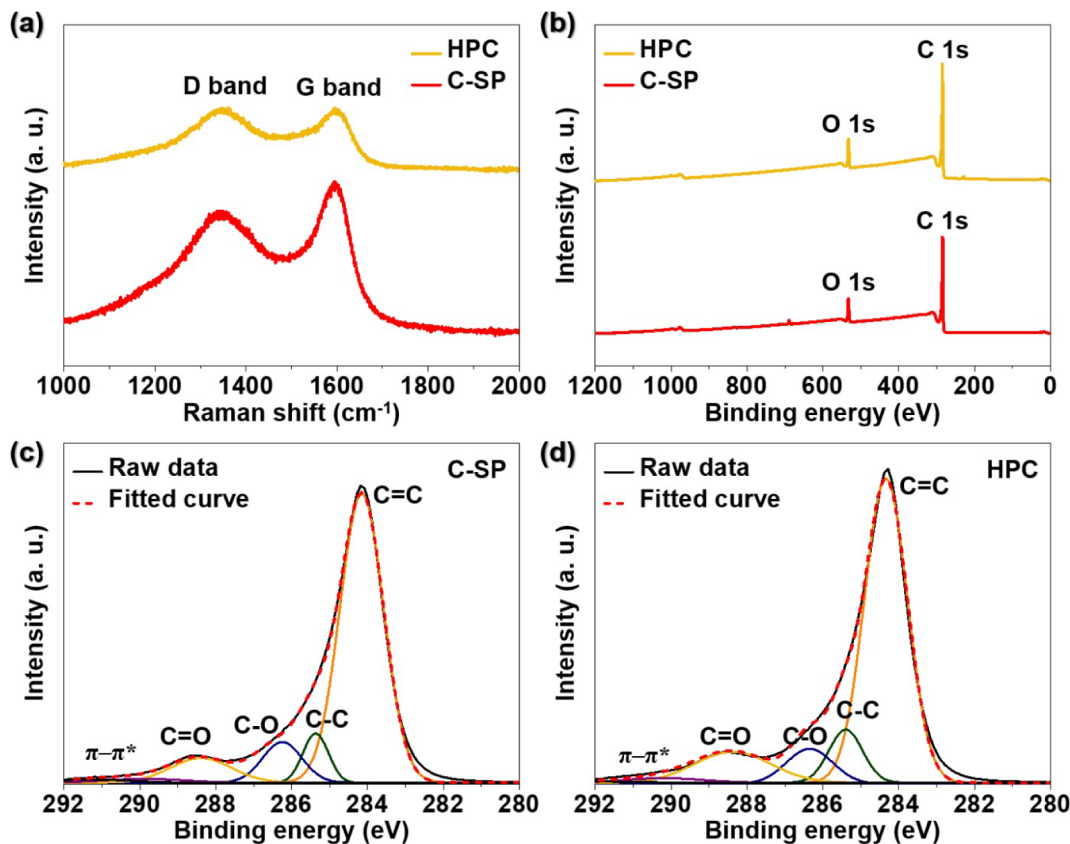


Fig. 7. Raman spectroscopy and XPS results of C-SP and HPC: (a) Raman spectra, (b) wide-scan XPS spectra, and C 1s spectra of (c) C-SP and (d) HPC.

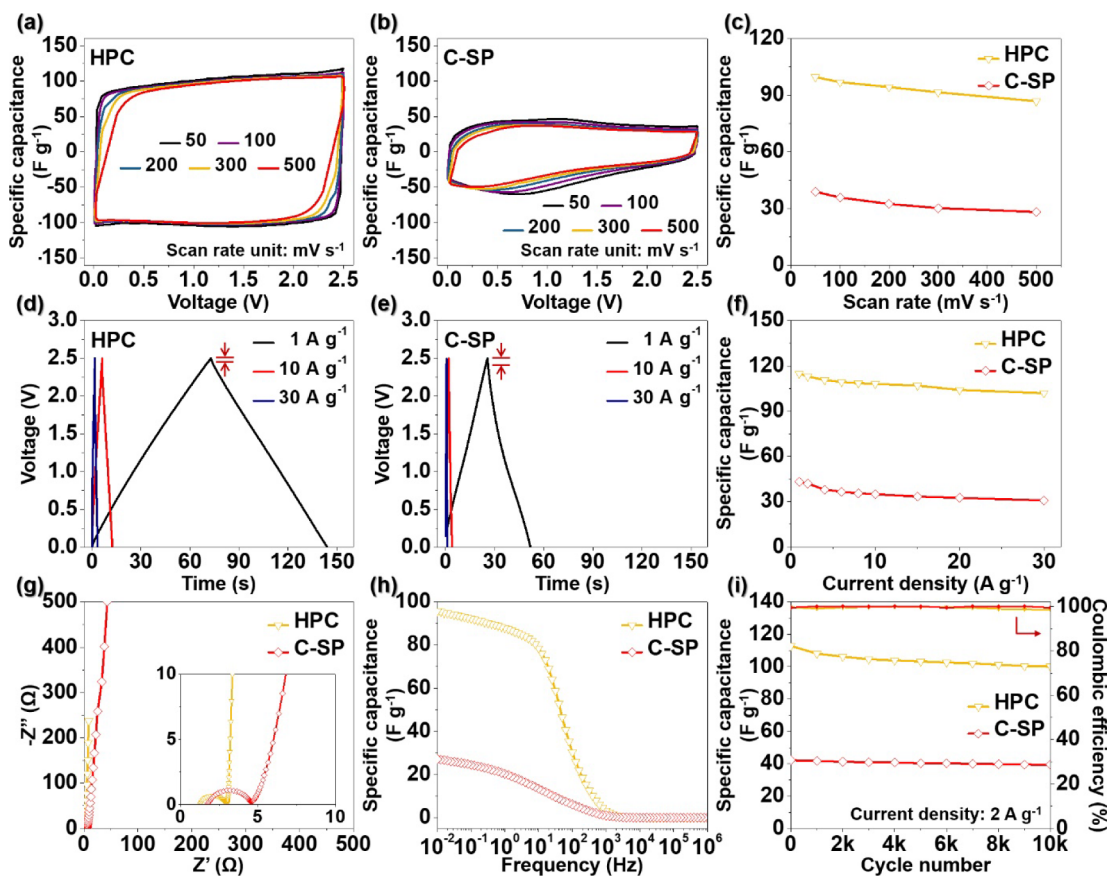


Fig. 8. Supercapacitor performances of HPC and C-SP in an organic electrolyte: (a) CV curves of HPC and (b) C-SP. (c) C_{sp} values of HPC and C-SP at different scan rates. GCD curves of (d) HPC and (e) C-SP. (f) C_{sp} values of HPC and C-SP at different current densities. (g) Nyquist plots and corresponding (h) C_{sp} -frequency plots of HPC and C-SP. (i) Cycling stability of HPC and C-SP at a current density of 2 A g^{-1} .

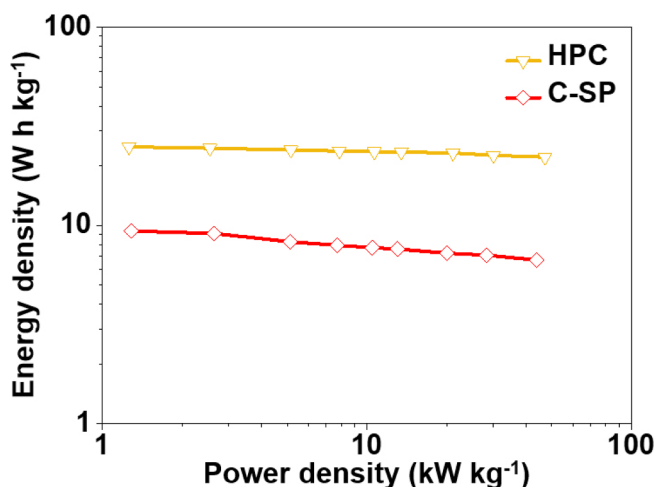


Fig. 9. Ragone plots of HPC and C-SP.

Acknowledgements

This research was supported by Basic Science Research Program through the National Research Foundation of Korea (NRF) funded by the Ministry of Education (2019R1A2C2088047).

Appendix A. Supplementary data

Supplementary data to this article can be found online at <https://doi.org/10.1016/j.cej.2019.122805>.

References

- [1] B.E. Conway, *Electrochemical Supercapacitors: Scientific Fundamentals and Technological Applications*, Kluwer Academic/Plenum Publishers, NY, USA, 1999.
- [2] H. Jiang, P.S. Lee, C. Li, 3D carbon based nanostructures for advanced supercapacitors, *Energy Environ. Sci.* 6 (2013) 41–53.
- [3] G. Wang, L. Zhang, J. Zhang, A review of electrode materials for electrochemical supercapacitors, *Chem. Soc. Rev.* 41 (2012) 797–828.
- [4] Q. Wang, J. Yan, Z. Fan, Carbon materials for high volumetric performance supercapacitors: design, progress, challenges and opportunities, *Energy Environ. Sci.* 9 (2016) 729–762.
- [5] A. González, E. Goikolea, J.A. Barrena, R. Mysyk, Review on supercapacitors: technologies and materials, *Renewable Sustainable Energy Rev.* 58 (2016) 1189–1206.
- [6] W. Raza, F. Ali, N. Raza, Y. Luo, K.-H. Kim, J. Yang, S. Kumar, A. Mahmood, E.E. Kwon, Recent advancements in supercapacitor technology, *Nano Energy* 52 (2018) 441–473.
- [7] G. Li, Z. Yang, Z. Yin, H. Guo, Z. Wang, G. Yan, Y. Liu, L. Li, J. Wang, Non-aqueous dual-carbon lithium-ion capacitors: a review, *J. Mater. Chem. A* 7 (2019) 15541–15563.
- [8] G. Li, Z. Yin, H. Guo, Z. Wang, G. Yan, Z. Yang, Y. Liu, X. Ji, J. Wang, Metalorganic quantum dots and their graphene-like derivative porous graphitic carbon for advanced lithium-ion hybrid supercapacitor, *Adv. Energy Mater.* 9 (2019) 1802878.
- [9] N. Yabuuchi, K. Kubota, M. Dahbi, S. Komaba, Research development on sodium-ion batteries, *Chem. Rev.* 114 (2014) 11636–11682.
- [10] J. Chmiola, G. Yushin, Y. Gogotsi, C. Portet, P. Simon, P.-L. Taberna, Anomalous increase in carbon capacitance at pore sizes less than 1 nanometer, *Science* 313 (2006) 1760–1763.
- [11] X. Wei, X. Jiang, J. Wei, S. Gao, Functional groups and pore size distribution do matter to hierarchically porous carbons as high-rate-performance supercapacitors, *Chem. Mater.* 28 (2016) 445–458.
- [12] H. Guo, B. Ding, J. Wang, Y. Zhang, X. Hao, L. Wu, Y. An, H. Dou, X. Zhang, Template-induced self-activation route for nitrogen-doped hierarchically porous carbon spheres for electric double layer capacitors, *Carbon* 136 (2018) 204–210.
- [13] L. Borchardt, D. Leistenschneider, J. Haase, M. Dvoyashkin, Revising the concept of pore hierarchy for ionic transport in carbon materials for supercapacitors, *Adv. Energy Mater.* 8 (2018) 1800892.
- [14] Y. Liang, F. Liang, H. Zhong, Z. Li, R. Fu, D. Wu, An advanced carbonaceous porous network for high-performance organic electrolyte supercapacitors, *J. Mater. Chem.*

- A 1 (2013) 7000–7005.
- [15] Z. Song, L. Li, D. Zhu, L. Miao, H. Duan, Z. Wang, W. Xiong, Y. Lv, M. Liu, L. Gan, Synergistic design of a N, O co-doped honeycomb carbon electrode and an ionogel electrolyte enabling all-solid-state supercapacitors with an ultrahigh energy density, *J. Mater. Chem. A* 7 (2019) 816–826.
- [16] Y. Li, Z. Li, P.K. Shen, Simultaneous formation of ultrahigh surface area and three-dimensional hierarchical porous graphene-like networks for fast and highly stable supercapacitors, *Adv. Mater.* 25 (2013) 2474–2480.
- [17] M. Rose, Y. Korenblit, E. Kockrick, L. Borchardt, M. Oschatz, S. Kaskel, G. Yushin, Hierarchical micro-and mesoporous carbide-derived carbon as a high-performance electrode material in supercapacitors, *Small* 7 (2011) 1108–1117.
- [18] V. Presser, M. Heon, Y. Gogotsi, Carbide-derived carbons – from porous networks to nanotubes and graphene, *Adv. Funct. Mater.* 21 (2011) 810–833.
- [19] A.B. Fuertes, M. Sevilla, Hierarchical microporous/mesoporous carbon nanosheets for high-performance supercapacitors, *ACS Appl. Mater. Interfaces* 7 (2015) 4344–4353.
- [20] H. Wang, Z. Xu, A. Kohandehghan, Z. Li, K. Cui, X. Tan, T.J. Stephenson, C.K. King'ondu, C.M. Holt, B.C. Olsen, J.K. Tak, D. Harfield, A.O. Anyia, D. Mitlin, Interconnected carbon nanosheets derived from hemp for ultrafast supercapacitors with high energy, *ACS Nano* 7 (2013) 5131–5141.
- [21] D. Zhu, J. Jiang, D. Sun, X. Qian, Y. Wang, L. Li, Z. Wang, X. Chai, L. Gan, M. Liu, A general strategy to synthesize high-level N-doped porous carbons via Schiff-base chemistry for supercapacitors, *J. Mater. Chem. A* 6 (2018) 12334–12343.
- [22] D. Xue, D. Zhu, M. Liu, H. Duan, L. Li, X. Chai, Z. Wang, Y. Lv, W. Xiong, L. Gan, Schiff-base/resin copolymer under hypersaline condition to high-level N-doped porous carbon nanosheets for supercapacitors, *ACS Appl. Nano Mater.* 1 (2018) 4998–5007.
- [23] Q. Ma, Y. Yu, M. Sindoro, A.G. Fane, R. Wang, H. Zhang, Carbon-based functional materials derived from waste for water remediation and energy storage, *Adv. Mater.* 29 (2017) 1605361.
- [24] T. Kim, G. Jung, S. Yoo, K.S. Suh, Activated graphene-based carbons as supercapacitor electrodes with macro-and mesopores, *ACS Nano* 7 (2013) 6899–6905.
- [25] Y.-J. Gu, W. Wen, J.-M. Wu, Simple air calcination affords commercial carbon cloth with high areal specific capacitance for symmetrical supercapacitors, *J. Mater. Chem. A* 6 (2018) 21078–21086.
- [26] S. Dong, X. He, H. Zhang, X. Xie, M. Yu, C. Yu, N. Xiao, J. Qiu, Surface modification of biomass-derived hard carbon by grafting porous carbon nanosheets for high-performance supercapacitors, *J. Mater. Chem. A* 6 (2018) 15954–15960.
- [27] P. Cheng, T. Li, H. Yu, L. Zhi, Z. Liu, Z. Lei, Biomass-derived carbon fiber aerogel as a binder-free electrode for high-rate supercapacitors, *J. Phys. Chem. C* 120 (2016) 2079–2086.
- [28] X. Chen, M. Chi, L. Xing, X. Xie, S. Liu, Y. Liang, M. Zheng, H. Hu, H. Dong, Y. Liu, S.P. Jiang, Y. Xiao, Natural plant template-derived cellular framework porous carbon as a high-rate and long-life electrode material for energy storage, *ACS Sustainable Chem. Eng.* 7 (2019) 5845–5855.
- [29] X. He, H. Zhang, H. Zhang, X. Li, N. Xiao, J. Qiu, Direct synthesis of 3D hollow porous graphene balls from coal tar pitch for high performance supercapacitors, *J. Mater. Chem. A* 2 (2014) 19633–19640.
- [30] J.H. Bang, K.S. Suslick, Applications of ultrasound to the synthesis of nanostructured materials, *Adv. Mater.* 22 (2010) 1039–1059.
- [31] D.S. Jung, Y.N. Ko, Y.C. Kang, S.B. Park, Recent progress in electrode materials produced by spray pyrolysis for next-generation lithium ion batteries, *Adv. Powder Technol.* 25 (2014) 18–31.
- [32] P. Nie, G. Xu, J. Jiang, H. Dou, Y. Wu, Y. Zhang, J. Wang, M. Shi, R. Fu, X. Zhang, Aerosol-spray pyrolysis toward preparation of nanostructured materials for batteries and supercapacitors, *Small Methods* 2 (2018) 1700272.
- [33] Y. Zhu, S.H. Choi, X. Fan, J. Shin, Z. Ma, M.R. Zachariah, J.W. Choi, C. Wang, Recent progress on spray pyrolysis for high performance electrode materials in lithium and sodium rechargeable batteries, *Adv. Energy Mater.* 7 (2017) 1601578.
- [34] F. Sun, J. Gao, X. Pi, L. Wang, Y. Yang, Z. Qu, S. Wu, High performance aqueous supercapacitor based on highly nitrogen-doped carbon nanospheres with unimodal mesoporosity, *J. Power Sources* 337 (2017) 189–196.
- [35] M. Kim, I. Oh, J. Kim, Hierarchical porous silicon carbide with controlled micropores and mesopores for electric double layer capacitors, *J. Power Sources* 282 (2015) 277–285.
- [36] H.-N. Kwon, G.D. Park, Y.C. Kang, K.C. Roh, Fabrication of bimodal micro-mesoporous amorphous carbon-graphitic carbon-reduced graphene oxide composite microspheres prepared by pilot-scale spray drying and their application in supercapacitors, *Carbon* 144 (2019) 591–600.
- [37] E.H. Jo, J.-H. Choi, S.-R. Park, C.M. Lee, H. Chang, H.D. Jang, Size and structural effect of crumpled graphene balls on the electrochemical properties for supercapacitor application, *Electrochim. Acta* 222 (2016) 58–63.
- [38] E.H. Jo, H.D. Jang, H. Chang, S.K. Kim, J.H. Choi, C.M. Lee, 3 D network-structured crumpled graphene/carbon nanotube/polyaniline composites for supercapacitors, *ChemSusChem* 10 (2017) 2210–2217.
- [39] C. Wang, Y. Wang, J. Graser, R. Zhao, F. Gao, M.J. O'Connell, Solution-based carbohydrate synthesis of individual solid, hollow, and porous carbon nanospheres using spray pyrolysis, *ACS Nano* 7 (2013) 11156–11165.
- [40] F. Sun, H. Wu, X. Liu, F. Liu, H. Zhou, J. Gao, Y. Lu, Nitrogen-rich carbon spheres made by a continuous spraying process for high-performance supercapacitors, *Nano Res.* 9 (2016) 3209–3221.
- [41] Y. Yoo, G.D. Park, Y.C. Kang, Carbon microspheres with micro- and mesopores synthesized via spray pyrolysis for high-energy-density, electrical-double-layer capacitors, *Chem. Eng. J.* 365 (2019) 193–200.
- [42] L.-Q. Mai, A. Minhas-Khan, X. Tian, K.M. Hercule, Y.-L. Zhao, X. Lin, X. Xu, Synergistic interaction between redox-active electrolyte and binder-free functionalized carbon for ultrahigh supercapacitor performance, *Nat. Commun.* 4 (2013) 2923.
- [43] N. Jo, J.-H. Choi, K.Y. Jung, Enhanced electrosorption capacitance of porous carbon particles synthesized by spray pyrolysis, *J. Electrochim. Soc.* 160 (2013) E84–E89.
- [44] B.H. Min, K.Y. Jung, Improved porosity and ionic sorption capacity of carbon particles prepared by spray pyrolysis from an aqueous sucrose/NaHCO₃/TEOS solution, *RSC Adv.* 7 (2017) 21314–21322.
- [45] P.H. Kim, K.Y. Jung, A new strategy of spray pyrolysis to prepare porous carbon nanosheets with enhanced ionic sorption capacity, *RSC Adv.* 6 (2016) 1686–1693.
- [46] D.S. Jung, T.H. Hwang, S.B. Park, J.W. Choi, Spray drying method for large-scale and high-performance silicon negative electrodes in Li-ion batteries, *Nano Lett.* 13 (2013) 2092–2097.
- [47] M.E. Fortunato, M. Rostam-Abadi, K.S. Suslick, Nanostructured carbons prepared by ultrasonic spray pyrolysis, *Chem. Mater.* 22 (2010) 1610–1612.
- [48] S.E. Skrabalak, K.S. Suslick, Porous carbon powders prepared by ultrasonic spray pyrolysis, *J. Am. Chem. Soc.* 128 (2006) 12642–12643.
- [49] J.K. Kim, S.-K. Park, J.-S. Park, Y.C. Kang, Uniquely structured composite microspheres of metal sulfides and carbon with cubic nanorooms for highly efficient anode materials for sodium-ion batteries, *J. Mater. Chem. A* 7 (2019) 2636–2645.
- [50] J.H. Choi, S.K. Park, Y.C. Kang, A salt-templated strategy toward hollow iron selenides-graphitic carbon composite microspheres with interconnected multicavities as high-performance anode materials for sodium-ion batteries, *Small* 15 (2019) 1803043.
- [51] H. Ying, S. Zhang, Z. Meng, Z. Sun, W.-Q. Han, Ultrasmall Sn nanodots embedded inside N-doped carbon microcages as high-performance lithium and sodium ion battery anodes, *J. Mater. Chem. A* 5 (2017) 8334–8342.
- [52] M. Zhang, C. Yu, Z. Ling, J. Yu, S. Li, C. Zhao, H. Huang, J. Qiu, A recyclable route to produce biochar with a tailored structure and surface chemistry for enhanced charge storage, *Green Chem.* 21 (2019) 2095–2103.
- [53] A.K. Peterson, D.G. Morgan, S.E. Skrabalak, Aerosol synthesis of porous particles using simple salts as a pore template, *Langmuir* 26 (2010) 8804–8809.
- [54] J.D. Atkinson, M.E. Fortunato, S.A. Dastgheib, M. Rostam-Abadi, M.J. Rood, K.S. Suslick, Synthesis and characterization of iron-impregnated porous carbon spheres prepared by ultrasonic spray pyrolysis, *Carbon* 49 (2011) 587–598.
- [55] L. Zhou, H. Cao, S. Zhu, L. Hou, C. Yuan, Hierarchical micro-/mesoporous N-and O-enriched carbon derived from disposable cashmere: A competitive cost-effective material for high-performance electrochemical capacitors, *Green Chem.* 17 (2015) 2373–2382.
- [56] Y. Gong, D. Li, C. Luo, Q. Fu, C. Pan, Highly porous graphitic biomass carbon as advanced electrode materials for supercapacitors, *Green Chem.* 19 (2017) 4132–4140.
- [57] J. Yang, H. Wu, M. Zhu, W. Ren, Y. Lin, H. Chen, F. Pan, Optimized mesopores enabling enhanced rate performance in novel ultrahigh surface area meso-/microporous carbon for supercapacitors, *Nano Energy* 33 (2017) 453–461.
- [58] P. Cheng, S. Gao, P. Zang, X. Yang, Y. Bai, H. Xu, Z. Liu, Z. Lei, Hierarchically porous carbon by activation of shiitake mushroom for capacitive energy storage, *Carbon* 93 (2015) 315–324.
- [59] J. Kaufman, S. Metin, D. Saperstein, Symmetry breaking in nitrogen-doped amorphous carbon: infrared observation of the Raman-active G and D bands, *Phys. Rev. B* 39 (1989) 13053.
- [60] J. Niu, R. Shao, M. Liu, J. Liang, Z. Zhang, M. Dou, Y. Huang, F. Wang, Porous carbon electrodes with battery-capacitive storage features for high performance Li-ion capacitors, *Energy Storage Mater.* 12 (2018) 145–152.
- [61] A. Primo, I. Esteve-Adell, J.F. Blandez, A. Dhakshinamoorthy, M. Álvaro, N. Candu, S.M. Coman, V.I. Parvulescu, H. García, High catalytic activity of oriented 2.0.0 copper(I) oxide grown on graphene film, *Nat. Commun.* 6 (2015) 8561.
- [62] V. Datsyuk, M. Kalyva, K. Papagelis, J. Parthenios, D. Tasis, A. Siokou, I. Kallitsis, C. Galiots, Chemical oxidation of multiwalled carbon nanotubes, *Carbon* 46 (2008) 833–840.
- [63] X. Wei, J.-S. Wei, Y. Li, H. Zou, Robust hierarchically interconnected porous carbons derived from discarded rhus typhina fruits for ultrahigh capacitive performance supercapacitors, *J. Power Sources* 414 (2019) 13–23.
- [64] J. Zhao, Y. Jiang, H. Fan, M. Liu, O. Zhuo, X. Wang, Q. Wu, L. Yang, Y. Ma, Z. Hu, Porous 3D few-layer graphene-like carbon for ultrahigh-power supercapacitors with well-defined structure-performance relationship, *Adv. Mater.* 29 (2017) 1604569.
- [65] J. Zhao, H. Lai, Z. Lyu, Y. Jiang, K. Xie, X. Wang, Q. Wu, L. Yang, Z. Jin, Y. Ma, J. Liu, Z. Hu, Hydrophilic hierarchical nitrogen-doped carbon nanocages for ultrahigh supercapacitive performance, *Adv. Mater.* 27 (2015) 3541–3545.
- [66] B.-A. Mei, O. Munteshary, J. Lau, B. Dunn, L. Pilon, Physical interpretations of Nyquist plots for EDLC electrodes and devices, *J. Phys. Chem. C* 122 (2017) 194–206.
- [67] F. Hekmat, B. Sohrabi, M.S. Rahamanifar, M.R. Vaezi, Supercapacitive properties of coiled carbon nanotubes directly grown on nickel nanowires, *J. Mater. Chem. A* 2 (2014) 17446–17453.
- [68] A. Laheäär, P. Przygocki, Q. Abbas, F. Béguin, Appropriate methods for evaluating the efficiency and capacitive behavior of different types of supercapacitors, *Electrochim. Commun.* 60 (2015) 21–25.
- [69] Y. Gogotsi, R.M. Penner, Energy storage in nanomaterials - capacitive, pseudocapacitive, or battery-like? *ACS Nano* 12 (2018) 2081–2083.
- [70] D. Zhang, J. Zhao, C. Feng, R. Zhao, Y. Sun, T. Guan, B. Han, N. Tang, J. Wang, K. Li, J. Qiao, J. Zhang, Scalable synthesis of hierarchical macropore-rich activated carbon microspheres assembled by carbon nanoparticles for high rate performance supercapacitors, *J. Power Sources* 342 (2017) 363–370.